Automatica 46 (2010) 204–210

Contents lists available at ScienceDirect

Automatica

journal homepage: www.elsevier.com/locate/automatica

Brief paper

# Geometric properties of partial least squares for process monitoring☆

Gang Li [a], S. Joe Qin [b,c,*], Donghua Zhou [a,*]

[a] Department of Automation, TNList, Tsinghua University, Beijing 100084, PR China

[b] The Mork Family Department of Chemical Engineering and Materials Science, University of Southern California, Los Angeles, CA 90089, USA

[c] Ming Hsieh Department of Electrical Engineering, University of Southern California, Los Angeles, CA 90089, USA

ARTICLE INFO

*Article history:*
Received 30 September 2008
Received in revised form
24 July 2009
Accepted 14 October 2009
Available online 18 November 2009

*Keywords:*
Partial least squares (PLS)
Weight-deflated PLS (W-PLS)
Simplified PLS (SIMPLS)
Process monitoring

ABSTRACT

Projection to latent structures or partial least squares (PLS) produces output-supervised decomposition on input **X**, while principal component analysis (PCA) produces unsupervised decomposition of input **X**. In this paper, the effect of output **Y** on the **X**-space decomposition in PLS is analyzed and geometric properties of the PLS structure are revealed. Several PLS algorithms are compared in a geometric way for the purpose of process monitoring. A numerical example and a case study are given to illustrate the analysis results.



## 1. Introduction

Multivariate statistical process monitoring (SPM) has been successfully used in the monitoring of different industrial processes over the past two decades, including chemicals, polymers, and microelectronics manufacturing. Multivariate statistical process control charts based on principal component analysis (PCA), projection to latent structures (PLS), and other data-based structures have received great success in practice (Kresta, MacGregor & Marlin, 1991; Qin, 2003; Wise & Gallagher, 1996; Xia, Howell & Thornhill, 2005). Besides, fault reconstruction and estimation can be performed based on the latent space of PCA (Dunia & Qin, 1998; Qin, 2003), which enhances the application of SPM significantly.

To monitor all the variations and abnormal situations of input measurements (**X**), one can perform a PCA decomposition on the **X**-space. However, a more important objective of process monitoring is to provide assurance of good product quality that is impacted by the process conditions. Quality variables (**Y**) are affected by the processing conditions reflected in the measured **X**-data and possibly additional unmeasured factors. The quality data **Y** are often difficult to measure, and often come very infrequently with significant measurement delays. To monitor variations in the process variables that are most relevant to quality variables (**Y**), one can perform PLS decomposition on **X**-space.

The basic concepts and algorithms of PLS can be found in the chemometrics literature (Di Ruscio, 2000; Hóskuldsson, 1988; Ter Braak & De Jong, 1998). PLS has been used in multivariate monitoring of process operating performance, which is almost exactly in the same way as PCA-based monitoring (Kresta et al., 1991). Several variants of PLS have been proposed for monitoring, such as multi-block PLS (MacGregor, Jaeckle, Kiparissides & Koutoudi, 1994), dynamic PLS (Lee, Han & Yoon, 2004), recursive PLS (Qin, 1998) and multi-phase PLS (Lu, Gao & Wang, 2004).

Although PLS-based monitoring has been used for a long time, the property of the latent space induced by PLS has not been analyzed for process monitoring. While PCA-based monitoring methods are well understood (e.g., Alcala & Qin, 2009), it is not clear how **Y** affects the decomposition of **X**-space and the outcome of process monitoring. Westerhuis, Gurden and Smilde (2000) proposed generalized $T^2$ and Q statistics for many latent variable models (including PLS). The structure they used can be regarded as the structure of simplified PLS (SIMPLS) (De Jong, 1993). However, it is still an open question as to which PLS algorithm is the most appropriate for process monitoring.

In this paper, we show geometrically the **X**-space decomposition supervised by **Y** using PLS relative to PCA. Then, we reveal the geometric property of the decomposition induced by PLS. It is made clear why and how PLS should be used in process monitoring. Three PLS algorithms are analyzed in detail and the most appropriate structure for monitoring is pointed out.

The remainder of this paper is organized as follows. Section 2 reviews the standard PLS algorithm and its properties. Then, we

☆ The material in this paper was not presented at any conference. This paper was recommended for publication in revised form by Associate Editor Denis Dochain under the direction of Editor Frank Allgöwer.

* Corresponding author.
*E-mail addresses:* sqin@usc.edu (S.J. Qin), zdh@tsinghua.edu.cn (D. Zhou).

0005-1098/$ – see front matter © 2009 Elsevier Ltd. All rights reserved.
doi:10.1016/j.automatica.2009.10.030

**Table 1**
**X**-deflated NIPALS algorithm (Dayal & MacGregor, 1997).

Center the columns of **X, Y** to zero mean and scale them to unit variance. Set $i = 1$ and $\mathbf{X}_1 = \mathbf{X}$.
1. Set $\mathbf{u}_i$ equal to any column of **Y**.
2. $\mathbf{w}_i = \mathbf{X}_i^{\mathrm{T}}\mathbf{u}_i / \|\mathbf{X}_i^{\mathrm{T}}\mathbf{u}_i\|$.
3. $\mathbf{t}_i = \mathbf{X}_i\mathbf{w}_i$.
4. $\mathbf{q}_i = \mathbf{Y}^{\mathrm{T}}\mathbf{t}_i / \mathbf{t}_i^{\mathrm{T}}\mathbf{t}_i$.
5. $\mathbf{u}_i = \mathbf{Y}\mathbf{q}_i$.

If $\mathbf{t}_i$ converges, go to Step 6, else return to Step 2.
6. $\mathbf{p}_i = \mathbf{X}_i^{\mathrm{T}}\mathbf{t}_i / \mathbf{t}_i^{\mathrm{T}}\mathbf{t}_i$.
7. $\mathbf{X}_{i+1} = \mathbf{X}_i - \mathbf{t}_i\mathbf{p}_i^{\mathrm{T}}$.

Set $i = i + 1$ and return to step 1. Terminate if $i > A$.

discuss the effect of **Y** on the **X**-space decomposition in Section 3. The geometric properties of PLS on **X**-space decomposition are discussed in Section 4. Other PLS variants are analyzed in a similar way. Following that, we discuss the monitoring problem using PLS and its variants in Section 5. Section 6 uses a numerical example and a case study to illustrate the analysis results. Finally, we present conclusions in the last section.

## 2. Projection to latent spaces (PLS)

Given an input matrix $\mathbf{X} \in \mathbb{R}^{n\times m}$ consisting of $n$ samples with $m$ process variables per sample, and an output matrix $\mathbf{Y} \in \mathbb{R}^{n\times p}$ with $p$ quality variables per sample, PLS projects (**X, Y**) to a low-dimensional space defined by a small number of latent variables $(\mathbf{t}_1, \ldots, \mathbf{t}_A)$ ($A$ is the PLS component number) as follows:

$$\begin{cases} \mathbf{X} = \mathbf{T}\mathbf{P}^{\mathrm{T}} + \mathbf{E} \\ \mathbf{Y} = \mathbf{T}\mathbf{Q}^{\mathrm{T}} + \mathbf{F} \end{cases} \tag{1}$$

where $\mathbf{T} = [\mathbf{t}_1, \ldots, \mathbf{t}_A]$ is the score matrix, $\mathbf{P} = [\mathbf{p}_1, \ldots, \mathbf{p}_A]$ is the loading matrix for **X** and $\mathbf{Q} = [\mathbf{q}_1, \ldots, \mathbf{q}_A]$ is the loading matrix for **Y**. **E** and **F** are the modeling residual of **X** and **Y**. The data matrices **X, Y** are usually scaled to unit variance and zero mean. A nonlinear iterative partial least-squares algorithm (NIPALS) to perform PLS is described in Table 1. The objective of PLS embedded in this algorithm is to find the solution of the following problem:

$$\begin{aligned} &\max \quad \mathbf{w}_i^{\mathrm{T}}\mathbf{X}_i^{\mathrm{T}}\mathbf{Y}_i\mathbf{q}_i \\ &s.t. \quad \|\mathbf{w}_i\| = 1, \|\mathbf{q}_i\| = 1 \end{aligned}$$

where $\mathbf{w}_i$, $\mathbf{q}_i$ are weight vectors that yield $\mathbf{t}_i = \mathbf{X}_i\mathbf{w}_i$ and $\mathbf{u}_i = \mathbf{Y}_i\mathbf{q}_i$, respectively. Denoting $\mathbf{W} = [\mathbf{w}_1, \ldots, \mathbf{w}_A]$, **T** cannot be calculated from **X** directly using **W**. Let

$$\mathbf{r}_1 = \mathbf{w}_1, \quad \mathbf{r}_i = \prod_{j=1}^{i-1}(\mathbf{I}_m - \mathbf{w}_j\mathbf{p}_j^{\mathrm{T}})\mathbf{w}_i, \quad i > 1 \tag{2}$$

and $\mathbf{R} = [\mathbf{r}_1, \ldots, \mathbf{r}_A]$. Then, the score matrix **T** can be computed from the original **X** as follows:

$$\mathbf{T} = \mathbf{X}\mathbf{R} \tag{3}$$

**P**, **R** and **W** have the following relationship (Dayal & MacGregor, 1997; De Jong, 1993):

$$\mathbf{R} = \mathbf{W}(\mathbf{P}^{\mathrm{T}}\mathbf{W})^{-1} \tag{4}$$

$$\mathbf{P}^{\mathrm{T}}\mathbf{R} = \mathbf{R}^{\mathrm{T}}\mathbf{P} = \mathbf{W}^{\mathrm{T}}\mathbf{W} = \mathbf{I}_A. \tag{5}$$

In the PLS literature, the case of a single output is referred to as PLS1 and that for multiple outputs is referred to as PLS2. When there are several output variables, performing PLS1 of each output separately does not give the same results as PLS2 of multiple outputs jointly. Since outputs from one process are usually interrelated, it is appropriate to use PLS2 to capture the interrelationship among the output variables.

## 3. The effect of Y on the X-space decomposition

Many researchers use the PCA-based monitoring techniques for PLS decomposition of the **X**-space. However, the PLS decomposition can be radically different from the PCA decomposition, which makes one wonder whether the PLS-based monitoring should be different from the PCA-based monitoring techniques. In this section, we demonstrate the impact of **Y** on the decomposition of **X**-space in general, and then visualize the result geometrically.

Suppose **X** has the following PCA decomposition:

$$\mathbf{X} = \mathbf{t}_1\mathbf{v}_1^{\mathrm{T}} + \cdots + \mathbf{t}_l\mathbf{v}_l^{\mathrm{T}} \tag{6}$$

where $\mathbf{v}_i$ $(1 \le i \le l)$ are the orthonormal eigenvectors related to nonzero eigenvalues of $\mathbf{X}^{\mathrm{T}}\mathbf{X}$, $\lambda_1 \ge \cdots \ge \lambda_l > 0$ and $l = rank(\mathbf{X}) \le m$. In PCA $\mathbf{v}_i$ $(1 \le i \le l)$ alone define the decomposition of the input space. In PLS however, the input space decomposition is defined by two matrices, **P** and **R**. Therefore, the angle between $\mathbf{r}_i$ and $\mathbf{p}_i$, unless it is zero, reflects the impact of **Y** on the decomposition of **X**-space in PLS. For the ease of presentation, we drop the subscript $i$ for the moment.

The PLS weight vector **r** is in Span$\{\mathbf{v}_1, \ldots, \mathbf{v}_l\}$ according to the properties of PLS. Therefore,

$$\mathbf{r} = r\sum_{i=1}^{l}\alpha_i\mathbf{v}_i \tag{7}$$

where $r = \|\mathbf{r}\|$ and

$$\sum_{i=1}^{l}\alpha_i^2 = 1. \tag{8}$$

Then,

$$\mathbf{p} = \mathbf{X}^{\mathrm{T}}\boldsymbol{t}/\boldsymbol{t}^{\mathrm{T}}\mathbf{t} = \frac{\mathbf{X}^{\mathrm{T}}\mathbf{X}\mathbf{r}}{\mathbf{t}^{\mathrm{T}}\mathbf{t}} = \frac{\sum_{i=1}^{l}\lambda_i\alpha_i\mathbf{v}_i}{r\sum_{i=1}^{l}\lambda_i\alpha_i^2}. \tag{9}$$

From (5), we have $\mathbf{r}^{\mathrm{T}}\mathbf{p} = 1$ for each dimension. Therefore,

$$\cos\angle(\mathbf{r}, \mathbf{p}) = \frac{1}{r\|\mathbf{p}\|} = \frac{\sum_{i=1}^{l}\lambda_i\alpha_i^2}{\sqrt{\sum_{i=1}^{l}\lambda_i^2\alpha_i^2}} \tag{10}$$

and

$$\max\angle(\mathbf{r}, \mathbf{p}) = \arccos\frac{2\sqrt{\lambda_1\lambda_l}}{\lambda_1 + \lambda_l}. \tag{11}$$

Result (11) is obtained by minimizing (10) subject to (8). The solution process is omitted due to page limitation.

Several points can be summarized about the effect of **Y** on PLS decomposition of the **X**-space.

(i) Generally, **r** and **p** in PLS have a nonzero angle.
(ii) $\angle(\mathbf{r}, \mathbf{p})$ has an upper bound determined by (11). This upper bound increases with the difference among $\lambda_i$.
(iii) If **r** is an eigenvector of $\mathbf{X}^{\mathrm{T}}\mathbf{X}$, all but one $\alpha_i$ is zero, which makes (10) equal to one and $\angle(\mathbf{r}, \mathbf{p}) = 0$.
(iv) If $\lambda_i$ are equal, $\angle(\mathbf{r}, \mathbf{p}) = 0$.

To visualize the results geometrically, consider the special case of two inputs and one output. Suppose $\mathbf{X} = [\mathbf{x}_1, \mathbf{x}_2] = \mathbf{t}_1\mathbf{v}_1^{\mathrm{T}} + \mathbf{t}_2\mathbf{v}_2^{\mathrm{T}} \in \mathbb{R}^{n\times 2}$, $\mathbf{y} = c_1\mathbf{t}_1 + c_2\mathbf{t}_2 \in \mathbb{R}^{n\times 1}$.Then, (11) reduces to

$$\max\angle(\mathbf{r}, \mathbf{p}) = \arccos\frac{2\sqrt{\lambda_1\lambda_2}}{\lambda_1 + \lambda_2}. \tag{12}$$

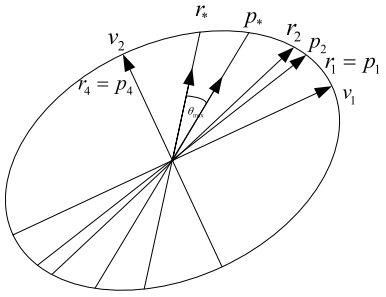


**Fig. 1.** Effect on **X**-space decomposition by **y**.

From (12), it can be observed that max $\angle(\mathbf{r}, \mathbf{p})$ is close to 0 when $\lambda_2$ is close to $\lambda_1$.

Fig. 1 describes different cases in a geometric way. In PCA, the **X**-space is decomposed by $\mathbf{v}_1$ and $\mathbf{v}_2$. In PLS, it depends on **X** and **y** jointly. If $c_2 = 0$, then **r** coincide with $\mathbf{v}_1$, which forms the same decomposition as PCA. $\mathbf{r}_1$ and $\mathbf{p}_1$ in Fig. 1 denote this case. If **y** is more related to $\mathbf{t}_2$ and less to $\mathbf{t}_1$, then **r** is chosen to be farther from $\mathbf{v}_1$ and closer to $\mathbf{v}_2$,which causes $\angle(\mathbf{r}, \mathbf{p})$ to increase. The case is described by $\mathbf{r}_2$, $\mathbf{p}_2$ in Fig. 1. The largest angle between vectors **r** and **p** are represented by $\mathbf{r}^*$, $\mathbf{p}^*$. If $c_1 = 0$, **y** is only related to $\mathbf{t}_2$, then **r** and **p** overlap again ($\mathbf{r} = \mathbf{p} = \mathbf{v}_2$), which are denoted by $\mathbf{r}_4$ and $\mathbf{p}_4$, respectively.

Therefore, the impact of Y on the decomposition of the **X**-space depends on how ellipsoidal the covariance of **X** is (i.e. unequal $\lambda_i$) and how much **Y** is correlated to the leading PCA scores of **X**. In typical engineering applications, **X** data are highly correlated. Therefore, the covariance of **X** is usually very ellipsoidal. As a consequence, the upper bound of $\angle(\mathbf{p}, \mathbf{r})$ can be significant. If **Y** is mostly correlated to the leading PCA scores of **X**, the PLS decomposition of the **X**-space is similar to the PCA decomposition of the **X**-space. In this case, the PCA monitoring techniques can be directly applied to the PLS model and residuals. If, on the other hand, **Y** is highly correlated to the non-leading PCA scores of **X**, the PLS decomposition of the **X**-space in (1) can be very different from the PCA decompositions of the **X**-space. The variance left in the **X**-residual (**E**) can be large and the direct application of Q statistic monitoring on the **X**-residual is questionable.

## 4. Geometric properties of PLS

### 4.1. Space decomposition of PCA

In PCA the input vector **x** is decomposed as follows (Qin, 2003):

$$\begin{aligned}&\mathbf{x} = \hat{\mathbf{x}} + \tilde{\mathbf{x}}\\ &\hat{\mathbf{x}} = \mathbf{P}\mathbf{P}^{\mathrm{T}}\mathbf{x} \in S_p \equiv \mathrm{Span}\{\mathbf{P}\}\\ &\tilde{\mathbf{x}} = (\mathbf{I} - \mathbf{P}\mathbf{P}^{\mathrm{T}})\mathbf{x} \in S_r \equiv \mathrm{Span}\{\mathbf{P}\}^{\perp}\end{aligned} \tag{13}$$

where **P** is the loading matrix of PCA, and $\mathrm{Span}\{\mathbf{P}\}^{\perp}$ is the orthogonal complement of $\mathrm{Span}\{\mathbf{P}\}$. $\mathbf{P}\mathbf{P}^{\mathrm{T}}$ and $\mathbf{I} - \mathbf{P}\mathbf{P}^{\mathrm{T}}$ are both orthogonal projectors. Thus, (13) is an orthogonal decomposition.

### 4.2. Space decomposition of PLS

From (5), we can easily obtain

$$(\mathbf{P}\mathbf{R}^{\mathrm{T}})^2 = \mathbf{P}\mathbf{R}^{\mathrm{T}}. \tag{14}$$

Thus, $\mathbf{P}\mathbf{R}^{\mathrm{T}}$ is an idempotent matrix. Generally speaking, $\mathbf{P}\mathbf{R}^{\mathrm{T}}$ is not symmetric. Therefore, $\mathbf{P}\mathbf{R}^{\mathrm{T}}$ is an oblique projector (Zhang, 2004).

**Lemma 1.** *Let $\boldsymbol{\Pi}_{P|R^{\perp}}$ denote the projector onto the subspace* $\mathrm{Span}\{\mathbf{P}\}$, *along the subspace* $\mathrm{Span}\{\mathbf{R}\}^{\perp}$.

$$\begin{aligned}&\boldsymbol{\Pi}_{P|R^{\perp}} = \mathbf{P}\mathbf{R}^{\mathrm{T}}\\ &\boldsymbol{\Pi}_{R^{\perp}|P} = \mathbf{I} - \mathbf{P}\mathbf{R}^{\mathrm{T}}.\end{aligned} \tag{15}$$

The proof is given in Appendix A.

From Lemma 1, we have the following theorem on the PLS decomposition:

**Theorem 1.** *PLS induces an oblique decomposition on input variable space:*

$$\begin{aligned}&\mathbf{x} = \hat{\mathbf{x}} + \tilde{\mathbf{x}}\\ &\hat{\mathbf{x}} = \mathbf{P}\mathbf{R}^{\mathrm{T}}\mathbf{x} \in S_p \equiv \mathrm{Span}\{\mathbf{P}\}\\ &\tilde{\mathbf{x}} = (\mathbf{I} - \mathbf{P}\mathbf{R}^{\mathrm{T}})\mathbf{x} \in S_r \equiv \mathrm{Span}\{\mathbf{R}\}^{\perp}.\end{aligned} \tag{16}$$

The theorem can be proven by noting from Lemma 1 that

$$\mathrm{Span}\{\mathbf{I} - \mathbf{P}\mathbf{R}^{\mathrm{T}}\} = \mathrm{Span}\{\mathbf{R}\}^{\perp}. \tag{17}$$

Different from PCA, $\hat{\mathbf{x}}$ is not orthogonal to $\tilde{\mathbf{x}}$ in PLS. Therefore, we conclude that in the PLS model, $\hat{\mathbf{x}}$ is the projection of **x** onto $\mathrm{Span}\{\mathbf{P}\}$ along $\mathrm{Span}\{\mathbf{R}\}^{\perp}$ and $\tilde{\mathbf{x}}$ is the projection of **x** onto $\mathrm{Span}\{\mathbf{R}\}^{\perp}$ along $\mathrm{Span}\{\mathbf{P}\}$.

### 4.3. Variants of PLS

The weight-deflated PLS (W-PLS) is a variant of PLS proposed by Helland (1988), which has the same prediction ability as the standard PLS. The relationships between W-PLS and PLS are as follows (Helland, 1988).

1. **W** in W-PLS is identical to **W** in the standard PLS.
2. $\mathrm{Span}\{\mathbf{T}\}$ in W-PLS is the same as $\mathrm{Span}\{\mathbf{T}\}$ in the standard PLS.

From (4), we know that **W** and **R** share the same column space, which means

$$\mathrm{Span}\{\mathbf{W}\} = \mathrm{Span}\{\mathbf{R}\}. \tag{18}$$

W-PLS induces the following input space decomposition,

$$\begin{aligned}&\mathbf{x} = \hat{\mathbf{x}}_w + \tilde{\mathbf{x}}_w\\ &\hat{\mathbf{x}}_w = \mathbf{W}\mathbf{W}^{\mathrm{T}}\mathbf{x} \in \mathrm{Span}\{\mathbf{R}\}\\ &\tilde{\mathbf{x}}_w = (\mathbf{I} - \mathbf{W}\mathbf{W}^{\mathrm{T}})\mathbf{x} \in \mathrm{Span}\{\mathbf{R}\}^{\perp}\end{aligned} \tag{19}$$

which is an orthogonal decomposition.

De Jong (1993) proposed SIMPLS as an alternative approach of PLS. SIMPLS is proven to be identical to PLS1 for one output, and different from PLS2 with multiple outputs (Ter Braak & De Jong, 1998).

A difference between PLS and SIMPLS is in which subspace to search for $\mathbf{w}_i$ and how to obtain $\mathbf{r}_i$. In PLS, $\mathbf{w}_i$ is found in $\mathrm{Span}\{\mathbf{R}_{i-1}\}^{\perp}$, and $\mathbf{r}_i$ is obtained by projecting $\mathbf{w}_i$ to $\mathrm{Span}\{\mathbf{P}_{i-1}\}^{\perp}$ along $\mathrm{span}\{\mathbf{R}_{i-1}\}$. In SIMPLS, $\mathbf{w}_i$ is found in $\mathrm{Span}\{\mathbf{P}_{i-1}\}^{\perp}$ directly and $\mathbf{r}_i = \mathbf{w}_i$, because $\mathbf{w}_i \in \mathrm{Span}\{\mathbf{P}_{i-1}\}^{\perp}$.

SIMPLS provides another decomposition of **X**-space as follows:

$$\begin{aligned}&\mathbf{x} = \hat{\mathbf{x}}_s + \tilde{\mathbf{x}}_s\\ &\hat{\mathbf{x}}_s = \mathbf{P}\mathbf{P}^{+}\mathbf{x} \in \mathrm{Span}\{\mathbf{P}\}\\ &\tilde{\mathbf{x}}_s = (\mathbf{I} - \mathbf{P}\mathbf{P}^{+})\mathbf{x} \in \mathrm{Span}\{\mathbf{P}\}^{\perp}\end{aligned} \tag{20}$$

where $\mathbf{P}^{+} = (\mathbf{P}^{\mathrm{T}}\mathbf{P})^{-1}\mathbf{P}^{\mathrm{T}}$ is the generalized inverse of **P**. $\mathbf{P}\mathbf{P}^{+}$ is the orthogonal projector on $\mathrm{Span}\{\mathbf{P}\}$, while $\mathbf{I} - \mathbf{P}\mathbf{P}^{+}$ is the orthogonal projector on $\mathrm{Span}\{\mathbf{P}\}^{\perp}$. Therefore, (20) is an orthogonal decomposition of the **X**-space.

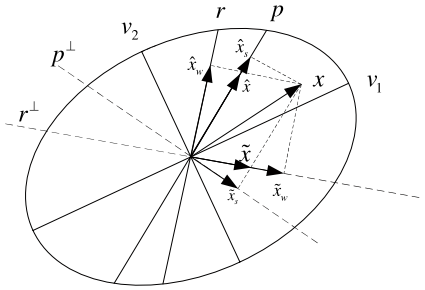


**Fig. 2.** Decompositions of PLS, W-PLS and SIMPLS.

### 4.4. Comparison of PLS, W-PLS, and SIMPLS

From (16), (19) and (20), it can be observed that W-PLS, SIMPLS and PLS are different in the decomposition of the **X**-space. We depict the decomposition results of PLS, W-PLS and SIMPLS in Fig. 2, where $\hat{\mathbf{x}}$ *and* $\tilde{\mathbf{x}}$ are from the standard PLS, while $\hat{\mathbf{x}}_w$ *and* $\tilde{\mathbf{x}}_w$ are from W-PLS, and $\hat{\mathbf{x}}_s$, $\tilde{\mathbf{x}}_s$ are from SIMPLS.

In PCA, both of the following relations hold:

$$\mathbf{T}^{\mathrm{T}}\tilde{\mathbf{X}} = 0 \tag{21}$$

$$\hat{\mathbf{x}}^{\mathrm{T}}\tilde{\mathbf{x}} = 0. \tag{22}$$

Relation (21) describes the orthogonality in the sample space, which guarantees that the scores extracted from **X** are uncorrelated to the residuals. Relation (22) describes the orthogonal decomposition in the variable space, which guarantees that $\hat{\mathbf{x}}$ and $\tilde{\mathbf{x}}$ are mutually exclusive. However, in the above PLS algorithms, only one of relations can be guaranteed at the same time. With an oblique projection, the scores are uncorrelated to the residuals but $\hat{\mathbf{x}}$ and $\tilde{\mathbf{x}}$ in the variable space are not orthogonal. With an orthogonal projection, $\hat{\mathbf{x}}$ and $\tilde{\mathbf{x}}$ are orthogonal, but the scores are correlated to residuals. In the next section, we reveal which PLS projection is the most appropriate for process monitoring.

## 5. Process monitoring with PLS

### 5.1. Monitoring with PLS

When a fault occurs, one or more measurement variables are affected, which breaks the normal relationship among these variables. PLS decomposes the measured data **X** into $S_r$ and $S_p$ subspaces, and fault detection is done by monitoring these subspaces.

If an abnormal situation affects quality **Y**, it is thought to happen in the $S_p$ subspace (MacGregor et al., 1994). Otherwise, if a fault has no impact on quality **Y**, it is thought to happen in the $S_r$ subspace. $T^2$ statistic is used to monitor faults in $S_p$, while $Q$ statistic is used to monitor faults in $S_r$. Therefore, PLS-based fault detection can tell whether a fault is related to the quality **Y**.

Given a new sample $\mathbf{x}_{new}$, the PLS score and residual can be calculated from (3) and (16):

$$\begin{aligned}\mathbf{t}_{new} &= \mathbf{R}^{\mathrm{T}}\mathbf{x}_{new}\\ \tilde{\mathbf{x}}_{new} &= (\mathbf{I} - \mathbf{P}\mathbf{R}^{\mathrm{T}})\mathbf{x}_{new}.\end{aligned} \tag{23}$$

Then, two statistics $T^2$ and Q are defined as follows:

$$\begin{aligned}T^2 &= \mathbf{t}_{new}^{\mathrm{T}}\boldsymbol{\Lambda}^{-1}\mathbf{t}_{new}\\ Q &= \|\tilde{\mathbf{x}}_{new}\|^2\end{aligned} \tag{24}$$

where $\boldsymbol{\Lambda} = \frac{1}{n-1}\mathbf{T}^{\mathrm{T}}\mathbf{T}$ is the sample covariance matrix of $\mathbf{t}$, $A$ is the number of PLS components, $n$ is the number of training samples. The control limits for these statistics are given in, for example, MacGregor et al. (1994) and Choi and Lee (2005). If $T^2$ and $Q$ are within the control limits, the process is normal. If $T^2$ exceeds the control limit, it is thought that there is a fault related to Y in the process. If $Q$ exceeds the control limit, it is thought that the fault is unrelated to Y.

### 5.2. Monitoring with SIMPLS

SIMPLS calculates the scores and residuals as follows:

$$\begin{aligned}\mathbf{t}_{s,new} &= \mathbf{P}^{+}\mathbf{x}_{new}\\ \tilde{\mathbf{x}}_{s,new} &= (\mathbf{I} - \mathbf{P}\mathbf{P}^{+})\mathbf{x}_{new},\end{aligned} \tag{25}$$

which has been used by Westerhuis et al. (2000). Statistics $T_s^2$ and $Q_s$ are defined similar to (24).

#### 5.2.1. Relation between $\mathbf{t}$ and $\mathbf{t}_s$

In order to describe the relation between them, the following lemma is introduced.

**Lemma 2.** *Let* $D_{\hat{\mathbf{x}}} = \hat{\mathbf{x}}^{\mathrm{T}}\boldsymbol{\Gamma}_{\hat{\mathbf{x}}}^{+}\hat{\mathbf{x}}$*,where* $\boldsymbol{\Gamma}_{\hat{\mathbf{x}}}^{+}$ *is the generalized inverse of* $\frac{1}{n-1}\hat{\mathbf{X}}^{\mathrm{T}}\hat{\mathbf{X}}$*, then*

$$D_{\hat{x}} = T^2 \tag{26}$$

where $T^2$ is defined in (24). Lemma 2 is proven in Appendix B. With this lemma, we can compare $\hat{\mathbf{x}}$ and $\hat{\mathbf{x}}_s$ in the variable space instead of comparing $\mathbf{t}$ and $\mathbf{t}_s$. According to (16) and (20), $\hat{\mathbf{x}}$ and $\hat{\mathbf{x}}_s$ are projections of $\mathbf{x}$ onto the same subspace, Span{**P**}, along Span{**R**}$^{\perp}$ and Span{**P**}$^{\perp}$, respectively. Score $\mathbf{t}$ reflects the variations correlated to **Y**, while $\mathbf{t}_s$ reflects only parts of variations correlated to **Y**.

#### 5.2.2. Relation between $\tilde{\mathbf{x}}$ and $\tilde{\mathbf{x}}_s$

From (16) and (20) we know that $\tilde{\mathbf{x}}_s$ and $\tilde{\mathbf{x}}$ are projections of $\mathbf{x}$ onto Span{**P**}$^{\perp}$ and Span{**R**}$^{\perp}$, respectively, along the same subspace Span{**P**}. Thus,

$$\tilde{\mathbf{x}}_{\mathbf{s}} = \boldsymbol{\Pi}_P^{\perp}\tilde{\mathbf{x}} \tag{27}$$

where $\Pi_P^{\perp}$ is the orthogonal projection onto Span{**P**}$^{\perp}$. If we use $Q = \|\tilde{\mathbf{x}}\|^2 \le \delta_\alpha^2$ as in PLS based monitoring ($\delta_\alpha^2$ is the control limit of $Q$), the control region is a hyper-sphere in Span{**R**}$^{\perp}$. When projected onto Span{**P**}$^{\perp}$, it becomes a hyper-ellipsoid in the Span{**P**}$^{\perp}$. If we use $Q_s = \|\tilde{\mathbf{x}}_s\|^2 \le \delta_{s,\alpha}^2$ ($\delta_{s,\alpha}^2$ is the control limit of $Q_s$) in SIMPLS based monitoring, the control region is a hyper-sphere in the Span{**P**}$^{\perp}$. The above differences can affect the monitoring results.

### 5.3. Monitoring with W-PLS

W-PLS calculates the scores and residuals as follows:

$$\begin{aligned}\mathbf{t}_{w,new} &= \mathbf{W}^{\mathrm{T}}\mathbf{x}_{new}\\ \tilde{\mathbf{x}}_{w,new} &= (\mathbf{I} - \mathbf{W}\mathbf{W}^{\mathrm{T}})\mathbf{x}_{new}.\end{aligned} \tag{28}$$

Statistics $T_w^2$ and $Q_w$ are defined similar to (24).

#### 5.3.1. Relation between $\mathbf{t}$ and $\mathbf{t}_w$

From (4),

$$\mathbf{W} = \mathbf{R}\mathbf{G} \tag{29}$$

where $\mathbf{G} = \mathbf{P}^{\mathrm{T}}\mathbf{W}$ is nonsingular. Substituting (29) into (28) and (24), and considering (23), we have

$$\boldsymbol{\Lambda}_w = \frac{1}{n-1}\mathbf{T}_w^{\mathrm{T}}\mathbf{T}_w = \mathbf{G}^{\mathrm{T}}\frac{1}{n-1}\mathbf{T}^{\mathrm{T}}\mathbf{T}\mathbf{G} = \mathbf{G}^{\mathrm{T}}\Lambda\mathbf{G} \tag{30}$$

and

$$T_w^2 = \mathbf{t}_w^{\mathrm{T}}\boldsymbol{\Lambda}_w^{-1}\mathbf{t}_w = \mathbf{t}^{\mathrm{T}}\mathbf{G}\boldsymbol{\Lambda}_w^{-1}\mathbf{G}^{\mathrm{T}}\mathbf{t} = \mathbf{t}^{\mathrm{T}}\boldsymbol{\Lambda}^{-1}\mathbf{t} = T^2. \tag{31}$$

Therefore, the monitoring results using $\mathbf{t}$ and $\mathbf{t}_w$ are the same.

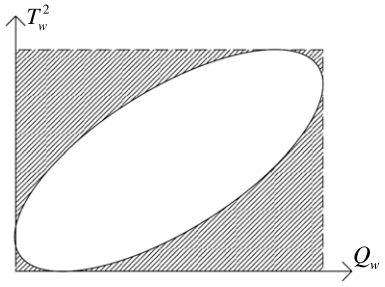


**Fig. 3.** Monitoring with $T_w^2$, $Q_w$ together.

**Table 2**
Properties of different monitoring policies.

| Monitoring policy | $\mathbf{T} \perp \tilde{\mathbf{X}}$ | $\hat{\mathbf{x}} \perp \tilde{\mathbf{x}}$ | $\mathbf{t}$ is $\mathbf{Y}$-related |
|---|---|---|---|
| PLS | Yes | No | Yes |
| W-PLS | No | Yes | Yes |
| SIMPLS | No | Yes | No |

### 5.3.2. Relation between $\tilde{\mathbf{x}}$ and $\tilde{\mathbf{x}}_w$

From (16) and (19), $\tilde{\mathbf{x}}$ and $\tilde{\mathbf{x}}_w$ are projections of $\mathbf{x}$ onto $\text{Span}\{\mathbf{R}\}^\perp$ along $\text{Span}\{\mathbf{P}\}$ and $\text{Span}\{\mathbf{R}\}$, respectively. Therefore, $Q$ and $Q_w$ monitor variabilities projected along different subspaces. The effect of these projections are studied later in this paper via simulation.

### 5.4. Comparison of three PLS monitoring policies

Table 2 shows properties of the PLS monitoring policies. The first and second properties are explained in (21) and (22). The third property describes whether $T^2$ explains $\mathbf{Y}$-related variations.

For monitoring using W-PLS, there are two shortcomings as $\tilde{\mathbf{x}}_w$ is correlated to $\mathbf{t}_w$. First, $Q_w$ will be affected by abnormal variations in $S_p$. Thus, it may cause reductant alarms in $Q_w$, even though the fault is in $S_p$ only, which makes it difficult to perform further fault diagnosis. Secondly, if we monitor process with $Q_w$ and $T_w^2$ together, the chance of failing to alarm will increase, which is shown in Fig. 3. Since $T_w^2$ and $Q_w$ are correlated, the normal condition should be located inside the ellipse, but the normal region defined by $T_w^2$ and $Q_w$ is rectangle. Therefore, if a faulty sample is located in the shaded area in Fig. 3, the W-PLS policy fails to alarm.

Similarly, monitoring using SIMPLS suffers from the same drawbacks. In addition, since $\mathbf{t}_s$ is not completely $\mathbf{Y}$-related, SIMPLS based monitoring loses the original purpose of PLS monitoring.

For monitoring using PLS, although $\hat{\mathbf{x}}$ is not orthogonal to $\tilde{\mathbf{x}}$, we can replace $\hat{\mathbf{x}}$ with $\hat{\mathbf{x}}_w$ according to Lemma 2 and (31) without any change of the monitoring results. From (16) and (20), it can be seen that $\hat{\mathbf{x}}_w \perp \tilde{\mathbf{x}}$. Thus, the standard PLS is the most appropriate for process monitoring among various algorithms.

## 6. Case study on simulation examples

### 6.1. A numerical example

Consider the following numerical example first:

$$\begin{cases} \mathbf{x}_k = \mathbf{A}\mathbf{z}_k + \mathbf{e}_k \\ y_k = \mathbf{C}\mathbf{x}_k + v_k \end{cases} \tag{32}$$

where $\mathbf{A} = \begin{pmatrix} 1 & 4 & 4 \\ 2 & 0 & 1 \end{pmatrix}^{\mathrm{T}}$, $\mathbf{z}_k \sim \mathbf{N}(\mathbf{0}, 0.5^2\mathbf{I}_2)$, $\mathbf{e}_k \sim \mathbf{N}(0, 0.05^2\mathbf{I}_3)$, $v_k \sim N(0, 0.05^2)$, $\mathbf{C} = \begin{pmatrix} 2 & 2 & 1 \end{pmatrix}$. The fault is added in the following form:

$$\mathbf{x}_k = \mathbf{x}_k^* + \boldsymbol{\Xi} f \tag{33}$$

**Table 3**
Fault occurs only in $S_p$.

| $f$ | Fault detection rates (%) | | | | | |
|---|---|---|---|---|---|---|
| | $T^2$ | $T_w^2$ | $T_s^2$ | $Q$ | $Q_w$ | $Q_s$ |
| 0 | 1.1 | 1.1 | 1.1 | 1.4 | 1.6 | 1.4 |
| 5 | 25.0 | 25.0 | 25.0 | 1.5 | 2.1 | 1.5 |
| std | 0.6 | 0.6 | 0.6 | 0.18 | 0.18 | 0.18 |
| 10 | 85.0 | 85.0 | 85.0 | 1.7 | 3.4 | 1.7 |
| std | 0.5 | 0.5 | 0.5 | 0.16 | 0.22 | 0.16 |
| 15 | 99.5 | 99.5 | 99.5 | 1.4 | 4.4 | 1.4 |
| std | 0.07 | 0.07 | 0.07 | 0.18 | 0.29 | 0.18 |
| 20 | 100 | 100 | 100 | 1.6 | 6.6 | 1.6 |
| std | 0.003 | 0.003 | 0.003 | 0.15 | 0.37 | 0.15 |
| 25 | 100 | 100 | 100 | 1.6 | 10.3 | 1.6 |
| std | 0 | 0 | 0 | 0.16 | 0.48 | 0.16 |

**Table 4**
Fault occurs only in $S_r$.

| $f$ | Fault detection rates (%) | | | | | |
|---|---|---|---|---|---|---|
| | $T^2$ | $T_w^2$ | $T_s^2$ | $Q$ | $Q_w$ | $Q_s$ |
| 0 | 1.2 | 1.2 | 1.2 | 1.5 | 1.5 | 1.5 |
| 2 | 1.3 | 1.3 | 1.3 | 32.5 | 31.4 | 32.5 |
| std | 0.17 | 0.17 | 0.16 | 0.76 | 0.71 | 0.76 |
| 4 | 1.0 | 1.0 | 0.9 | 96.4 | 95.9 | 96.4 |
| std | 0.17 | 0.17 | 0.17 | 0.27 | 0.27 | 0.27 |
| 6 | 1.0 | 1.0 | 1.0 | 100 | 100 | 100 |
| std | 0.17 | 0.17 | 0.16 | 0 | 0 | 0 |
| 8 | 1.0 | 1.0 | 1.0 | 100 | 100 | 100 |
| std | 0.17 | 0.17 | 0.16 | 0 | 0 | 0 |
| 100 | 1.2 | 1.2 | 7.9 | 100 | 100 | 100 |
| std | 0.15 | 0.15 | 0.40 | 0 | 0 | 0 |

where $\mathbf{x}^*$ is the normal value produced by (32), $\boldsymbol{\Xi}$ is the fault direction vector, and $f$ is the fault magnitude.

We use 100 samples under normal operation condition to perform a PLS model with one component. Given a fault direction and magnitude, 50 faulty samples per batch are produced according to (33) for fault detection. One hundred Monte Carlo simulations are performed to obtain the fault detection rates for PLS, WPLS and SIMPLS. The confidence of control limits is set to 99%. In order to show the efficiency of the comparison, we repeat the above procedure for 100 times and calculate the standard deviations of the detection rates, denoted by 'std' in the results.

#### 6.1.1. Fault occurs in $S_p$ only

Let $\boldsymbol{\Xi}_1 = [0.2500, 0.6641, 0.7046]^{\mathrm{T}} \in \text{Span}(\mathbf{P})$, where $\|\boldsymbol{\Xi}_1\| = 1$. Thus, the fault occurs in $S_p$ only. Table 3 shows the detection rates with fault magnitudes from 0 to 25.

From Table 3, it is observed that as the fault magnitude grows, the detection rates by $T^2$, $T_s^2$, $T_w^2$ increase, up to 100%. $Q$ and $Q_s$ are not affected by this fault, while $Q_w$ alarms redundantly. $Q_s$ has the same result as $Q$, which indicates the overlapped part monitored by $T_s^2$ and $Q_s$ is not affected by this fault. 'std' is the standard deviation of the estimated fault detection rate. From Table 3, it is observed that the differences among detection rates are significant compared to the corresponding standard deviations.

#### 6.1.2. Fault occurs in $S_r$ only

Let $\boldsymbol{\Xi}_2 = [0.9582, -0.1931, -0.2111]^{\mathrm{T}} \in \text{Span}(\mathbf{R})^\perp$, where $\|\boldsymbol{\Xi}_2\| = 1$. Thus, the fault occurs in $S_r$ only. Table 4 shows the fault detection rates of this fault with fault magnitudes from 0 to 8 and 100.

From Table 4, we observe that $T^2$ and $T_w^2$ are not affected by this fault. When fault magnitude is very large, $T_s^2$ is affected. This is because $\mathbf{t}_s$ is correlated to $\tilde{\mathbf{x}}_s$. However, $T_w^2$ is identical to $T^2$ in the monitoring as analyzed above, which indicates that the overlapped part monitored by $T_w^2$ and $Q_w$ is normal under this fault. It is also

**Table 5**
TEP case study.

| IDV | Fault detection rates (%) | | | | | | | | |
|---|---|---|---|---|---|---|---|---|---|
| | $T^2$ | $T_w^2$ | $T_s^2$ | $Q$ | $Q_w$ | $Q_s$ | $T^2+Q$ | $T_w^2+Q_w$ | $T_s^2+Q_s$ |
| 0 | 3.0 | 3.0 | 1.9 | 2.9 | 2.6 | 2.5 | 5.6 | 5.5 | 4.4 |
| 2 | 97.6 | 97.6 | 96.6 | 98.3 | 98.3 | 98.3 | 98.5 | 98.5 | 98.3 |
| 6 | 99.5 | 99.5 | 99.3 | 100 | 100 | 100 | 100 | 100 | 100 |
| 8 | 95.5 | 95.5 | 93.0 | 96.8 | 96.8 | 96.8 | 97.6 | 97.6 | 97.5 |
| 12 | 97.6 | 97.6 | 96.7 | 98.3 | 97.8 | 98.3 | 99.1 | 99.1 | 98.8 |
| 3 | 2.3 | 2.3 | 1.8 | 2.8 | 1.5 | 2.3 | 4.6 | 3.8 | 3.8 |
| 9 | 5.4 | 5.4 | 3.9 | 6.4 | 5.5 | 6.3 | 11.3 | 10.5 | 9.8 |
| 11 | 29.0 | 29.0 | 16.6 | 64.6 | 61.1 | 64.5 | 68.1 | 64.8 | 66.3 |
| 15 | 4.1 | 4.1 | 3.3 | 2.0 | 1.2 | 1.7 | 6.1 | 5.3 | 5.1 |

observed that as the fault magnitude grows, the detection rates by $Q$, $Q_s$, $Q_w$ increase, and $Q_w$ has a lower detection rate than $Q$ and $Q_s$. The difference among detection rates is significant considering their standard deviations from Table 4.

#### 6.1.3. Summary on the numerical example

The comparison of detection rates for faults in both $S_y$ and $S_r$ is not included due to page limitation, which has a similar result to the case study in the next subsection.

For all nonzero fault magnitudes, fault detection rates also reflect missing alarm rates. Further, the detection rates for zero fault magnitude correspond to the false alarm rates. From Tables 3 and 4, it can be observed that the false alarm rates for three policies are nearly the same.

### 6.2. Case study on TEP

In order to illustrate our point of view further, we use the Tennessee Eastman Process (TEP) as a case study (Downs & Vogel, 1993). The process is operated under closed-loop control. TEP has been widely used as a benchmark process for evaluating the process diagnosis methods such as PCA, multi-way PCA, and Fisher discriminant analysis (FDA) (Chiang, Russell & Braatz, 2001). PLS-based method has also been applied to the TEP (Lee et al., 2004). The TEP contains two blocks of variables: 12 manipulated variables and 41 measured variables (Chiang et al., 2001; Lee et al., 2004). Manipulated variables and process measurements are sampled with interval of 3 min. 19 composition measurements are sampled with time delays that vary from 6 min to 15 min. This time delay has a potentially critical impact on product quality control within the plant, which implies that the fault effect on product quality cannot be detected until the next sample of $\mathbf{Y}$ is available.

In this study, the composition of G in Stream 9 is chosen as the quality variable $\mathbf{y}$ with a time delay of 6 min. 22 process measurements and 11 manipulated variables are chosen as $\mathbf{X}$. There are 15 types of known faults in TEP, which are represented as IDV1-15. The detailed definition of $\mathbf{X}$, $\mathbf{y}$ variables and all the faults can be found in Chiang et al. (2001). First, 480 normal samples are centered to zero mean and scaled to unit variance to built a PLS with $A = 6$. Then, 800 faulty samples for each fault are used for fault detection based on three policies. The fault detection rates for several typical faults are listed in Table 5.

In Table 5, IDV 0 is normal data and the corresponding detection rate is the false alarm rate. IDV 2,6,8,12 are the faults related to quality data $\mathbf{y}$, and IDV 3,9,11,15 are the faults unrelated to quality data $\mathbf{y}$ (Zhou, Li & Qin, 2009). '+' means logical connection 'or'. From Table 5, we can find that PLS is more sensitive to detect the faults related to quality data $\mathbf{y}$, which is the purpose of monitoring with PLS. It is also observed that standard PLS has higher detection rates than W-PLS and SIMPLS in these simulated cases.

## 7. Conclusions

PLS has been widely used for monitoring complex industrial processes when quality variables are taken into account. There is, however, a lack of understanding of PLS geometry for the purpose of process monitoring. In this paper, the effect of $\mathbf{Y}$ on the decomposition of the $\mathbf{X}$-space is clearly shown and the geometric interpretation of the PLS decomposition structure is given. Based on this interpretation, two alternative algorithms of PLS, W-PLS and SIMPLS, are compared with the standard PLS in terms of the latent space decomposition and process monitoring. It is demonstrated that orthogonal sample space decomposition achieved by PLS is critical for process monitoring. It is concluded from analysis and simulation that monitoring using W-PLS and SIMPLS will cause ambiguous alarms and more missed alarms than the standard PLS. The standard PLS is the most appropriate for process monitoring among these alternative algorithms.

## Acknowledgements

This work was supported by the national 973 projects under Grants 2010CB731800 and 2009CB32602, and NSFC under Grants 60721003 and 60736026, and the Changjiang Professorship (S. Joe Qin) by the Ministry of Education of PR China.

## Appendix A. Proof of Lemma 1

According to Zhang (2004), the oblique projector onto Span($\mathbf{H}$) along Span($\mathbf{S}$) can be obtained by the following equation generally:

$$\boldsymbol{\Pi}_{H|S} = \mathbf{H}(\mathbf{H}^{\mathrm{T}}\boldsymbol{\Pi}_S^{\perp}\mathbf{H})^{-1}\mathbf{H}^{\mathrm{T}}\boldsymbol{\Pi}_S^{\perp} \tag{A.1}$$

where $\boldsymbol{\Pi}_S^{\perp}$ is the orthogonal projector onto the Span$(S)^{\perp}$. Noting that

$$\boldsymbol{\Pi}_{R^{\perp}}^{\perp} = \boldsymbol{\Pi}_R = \mathbf{R}(\mathbf{R}^{\mathrm{T}}\mathbf{R})^{-1}\mathbf{R}^{\mathrm{T}}. \tag{A.2}$$

Substituting (A.2) into (A.1) and considering (5), $\mathbf{R}$ is full-column-ranked, we can obtain

$$\boldsymbol{\Pi}_{P|R^{\perp}} = \mathbf{P}\mathbf{R}^{\mathrm{T}}. \tag{A.3}$$

Similarly, we have

$$\boldsymbol{\Pi}_{R^{\perp}|P} = \mathbf{I} - \mathbf{P}\mathbf{R}^{\mathrm{T}}. \tag{A.4}$$

Lemma 1 is proven. □

## Appendix B. Proof of Lemma 2

For a new sample $\mathbf{x}_{new}$, expanding $T^2$ and $D_{\hat{x}}$, we have

$$T^2 = \mathbf{x}_{new}^{\mathrm{T}}\mathbf{R}\boldsymbol{\Lambda}^{-1}\mathbf{R}^{\mathrm{T}}\mathbf{x}_{new} \tag{B.1}$$

$$D_{\hat{x}} = \mathbf{x}_{new}^{\mathrm{T}}\mathbf{R}\mathbf{P}^{\mathrm{T}}(\mathbf{P}\boldsymbol{\Lambda}\mathbf{P}^{\mathrm{T}})^{-}\mathbf{P}\mathbf{R}^{\mathrm{T}}\mathbf{x}_{new}. \tag{B.2}$$

As $\mathbf{P}$ is a full-column-ranked matrix, there exist two orthonormal matrix $\mathbf{U} \in \mathbb{R}^{m\times m}$, $\mathbf{V} \in \mathbb{R}^{A\times A}$, so that

$$\mathbf{P}^{\mathrm{T}} = \mathbf{V}[\boldsymbol{\Sigma}, \mathbf{O}]\mathbf{U}^{\mathrm{T}} \tag{B.3}$$

where $\boldsymbol{\Sigma}$ is a nonsingular diagonal matrix, and $\mathbf{O}$ is a zero matrix. Then, we have

$$\begin{aligned}
&\mathbf{P}^{\mathrm{T}}(\mathbf{P}\boldsymbol{\Lambda}\mathbf{P}^{\mathrm{T}})^{-}\mathbf{P}\\
&= \mathbf{V}[\boldsymbol{\Sigma}, \mathbf{O}]\mathbf{U}^{\mathrm{T}}(\mathbf{P}\boldsymbol{\Lambda}\mathbf{P}^{\mathrm{T}})^{-}\mathbf{U}[\boldsymbol{\Sigma}, \mathbf{O}]^{\mathrm{T}}\mathbf{V}^{\mathrm{T}}\\
&= \mathbf{V}[\boldsymbol{\Sigma}, \mathbf{O}]([\boldsymbol{\Sigma}, \mathbf{O}]^{\mathrm{T}}\mathbf{V}^{\mathrm{T}}\boldsymbol{\Lambda}\mathbf{V}[\boldsymbol{\Sigma}, \mathbf{O}])^{-}[\boldsymbol{\Sigma}, \mathbf{O}]^{\mathrm{T}}\mathbf{V}^{\mathrm{T}}\\
&= \mathbf{V}[\boldsymbol{\Sigma}, \mathbf{O}]\begin{bmatrix}(\boldsymbol{\Sigma}\mathbf{V}^{\mathrm{T}}\boldsymbol{\Lambda}\mathbf{V}\boldsymbol{\Sigma})^{-1} & \mathbf{O}\\ \mathbf{O} & \mathbf{O}\end{bmatrix}[\boldsymbol{\Sigma}, \mathbf{O}]^{\mathrm{T}}\mathbf{V}^{\mathrm{T}}\\
&= \mathbf{V}\boldsymbol{\Sigma}(\boldsymbol{\Sigma}\mathbf{V}^{\mathrm{T}}\boldsymbol{\Lambda}\mathbf{V}\boldsymbol{\Sigma})^{-1}\boldsymbol{\Sigma}\mathbf{V}^{\mathrm{T}} = \boldsymbol{\Lambda}^{-1}.
\end{aligned} \tag{B.4}$$

Lemma 2 is proven. □

## References


Alcala, C., & Qin, S. (2009). Reconstruction-based contribution for process monitoring. *Automatica*, *45*(7), 1593–1600.

Chiang, L. H., Russell, E., & Braatz, R. D. (2001). *Fault detection and diagnosis in industrial systems*. London: Springer.

Choi, S. W., & Lee, I. B. (2005). Multiblock PLS-based localized process diagnosis. *Journal of Process Control*, *15*(3), 295–306.

Dayal, B. S., & MacGregor, J. F. (1997). Improved PLS algorithms. *Journal of Chemometrics*, *11*(1), 73–85.

De Jong, S. (1993). SIMPLS: An alternative approach to partial least squares regression. *Chemometrics and Intelligent Laboratory Systems*, *18*(3), 251–263.

Di Ruscio, D. (2000). A weighted view on the partial least-squares algorithm. *Automatica*, *36*(6), 831–850.

Downs, J. J., & Vogel, E. F. (1993). A plant-wide industrial process control problem. *Computers & Chemical Engineering*, *17*(3), 245–255.

Dunia, R., & Qin, S. J. (1998). Subspace approach to multidimensional fault identification and reconstruction. *AIChE Journal*, *44*(8), 1813–1831.

Helland, I. S. (1988). On the structure of partial least squares regression. *Communications in Statistics-Simulation and Computation*, *17*(2), 581–607.

Hóskuldsson, A. (1988). PLS regression methods. *Journal of Chemometrics*, *2*, 211–228.

Kresta, J. V., MacGregor, J. F., & Marlin, T. E. (1991). Multivariate statistical monitoring of process operating performance. *Canadian Journal of Chemical Engineering*, *69*(1), 35–47.

Lee, G., Han, C. H., & Yoon, E. S. (2004). Multiple-fault diagnosis of the Tennessee Eastman process based on system decomposition and dynamic PLS. *Industrial and Engineering Chemistry Research*, *43*(25), 8037–8048.

Lu, N., Gao, F., & Wang, F. (2004). Sub-PCA modeling and on-line monitoring strategy for batch processes. *AIChE Journal*, *50*(1), 255–259.

MacGregor, J. F., Jaeckle, C., Kiparissides, C., & Koutoudi, M. (1994). Process monitoring and diagnosis by multiblock PLS methods. *AIChE Journal*, *40*(5), 826–838.

Qin, S. J. (1998). Recursive PLS algorithms for adaptive data modeling. *Computers and Chemical Engineering*, *22*(4–5), 503–514.

Qin, S. J. (2003). Statistical process monitoring: Basics and beyond. *Journal of Chemometrics*, *17*(8–9), 480–502.

Ter Braak, C. J. F., & De Jong, S. (1998). The objective function of partial least squares regression. *Journal of Chemometrics*, *12*(1), 41–54.

Westerhuis, J. A., Gurden, S. P., & Smilde, A. K. (2000). Generalized contribution plots in multivariate statistical process monitoring. *Chemometrics and Intelligent Laboratory Systems*, *51*(1), 95–114.

Wise, B. M., & Gallagher, N. B. (1996). The process chemometrics approach to process monitoring and fault detection. *Journal of Process Control*, *6*, 329–348.

Xia, C., Howell, J., & Thornhill, N. (2005). Detecting and isolating multiple plant-wide oscillations via spectral independent component analysis. *Automatica*, *41*(12), 2067–2075.

Zhang, X. D. (2004). *Matrix analysis and applications*. Beijing: Tsinghua University Press.

Zhou, D.H., Li, G., & Qin, S.J. (2009). Total projection to latent structures for process monitoring, *AIChE Journal*, published online, doi:10.1002/aic.11977.


**Gang Li** received his bachelor degree from the Department of Precision Instruments and Mechanology, Tsinghua University in 2004. He is now a Ph.D. candidate in the Department of Automation at Tsinghua University, Beijing, China. His research interest covers multivariate statistical process monitoring, and data-driven fault diagnosis and prognosis.

**S. Joe Qin** is the Fluor Professor at the Viterbi School of Engineering at University of Southern California and Chang Jiang Professor affiliated with Tsinghua University by the Ministry of Education of China. Prior to joining USC he held the Paul D. and Betty Robertson Meek and American Petrofina Foundation Centennial Professorship in Chemical Engineering at University of Texas at Austin. He obtained his B.S. and M.S. degrees in Automatic Control from Tsinghua University in Beijing, China, in 1984 and 1987, respectively, and his Ph.D. degree in Chemical Engineering from University of Maryland at College Park in 1992. He worked as a Principal Engineer at Fisher-Rosemount from 1992 to 1995.

Dr. Qin's research interests include statistical process monitoring and fault diagnosis, model predictive control, system identification, run-to-run control, semiconductor process control, and control performance monitoring. He is a Co-Director of the Texas–Wisconsin–California Control Consortium where he has been principal investigator for 14 years. He is a recipient of the National Science Foundation CAREER Award, DuPont Young Professor Award, Halliburton/Brown & Root Young Faculty Excellence Award, NSF-China Outstanding Young Investigator Award, and an IFAC Best Paper Prize for the model predictive control survey paper published in *Control Engineering Practice*. He is currently an Associate Editor for *Journal of Process Control* and *IEEE Transactions on Industrial Informatics*, and a Member of the Editorial Board for *Journal of Chemometrics*. He served as an Editor for *Control Engineering Practice* and an Associate Editor for *IEEE Transactions on Control Systems Technology*.

**Donghua Zhou** received his B.Eng., M.Sci., and Ph.D. degrees all from the Department of Electrical Engineering, Shanghai Jiaotong University, in 1985, 1988, and 1990, respectively. He was an Alexander von Humboldt Research Fellow (1995–1996) in the University of Duisburg, Germany, and a visiting scholar at Yale University (July 2001–Jan. 2002). Dr. Zhou is currently a Professor in the Department of Automation, Tsinghua University.

Dr. Zhou has published over 70 international journal papers and three monographs in the areas of process identification, diagnosis, and control. He serves the profession in many capacities such as IFAC Technical Committee on Fault Diagnosis and Safety of Technical Processes, associate editor of Journal of Process Control, Deputy General Secretary of Chinese Association of Automation (CAA), and Council member of CAA. He was also the NOC Chair of the 6th IFAC Symposium on SAFEPROCESS, 2006.